On Accretion Disks around a Black Hole and a Magnetized Neutron Star(Dissertation_全文)

AUTHOR(S):

Okuda, Toru

学位申請論文

奥田亨

On Accretion Disks around a Black Hole and a Magnetized Neutron Star

Tōru OKUDA
Institute of Earth Science, Hakodate College, Hokkaido University of Education, Hachiman-cho, Hakodate 040

Abstract

In order to examine whether stationary accretion disks around a black hole and a magnetized neutron star exist or not, we solve time-dependent hydrodynamical equations governing the mass, momentum, angular momentum, and energy conservations integrated over the thickness of the disk, under the assumption that vertical structure of the disk is given by a polytrope. Time integration of the equations starts with an initial state based on the standard accretion disk model.

The numerical results show that the accretion disks around the black hole and the magnetized neutron star except for the latter with a low accretion rate are thermally unstable in the inner region of the disks. The disks deviate significantly from the standard accretion disk model near the inner edge of the disk due to the effect of pressure gradient force and its coupling with angular momentum through viscous stress and evolve toward radiation pressure dominant, geometrically thick, but optically thin state with central disk parameters of lower densities and slightly incre-

ased temperatures, and finally a strong instability developes near the inner edge of the disk on the thermal time scale. The results show that the effect of the pressure gradient force can not be neglected in the stability analysis of the accretion disk, especially near the inner edge of the disk even if the disk is thin.

Key words : Accretion disk; Black hole; Magnetized neutron star; Thermal instability.

1. Introduction

Accretion disk around a compact star has been thought to play an important role in various X-ray sources. The accretion disk is likely to be formed when the compact star is a member of a close binary system and matter transferred from a giant type star onto its compact companion has high angular momentum.

Following the pioneer works by Pringle and Rees (1972), Shakura and Sunyaev (1973), and Novikov and Thorne (1973), a number of theoretical studies on the accretion disk have been developed to account for observations of the X-ray sources, particularly Cyg X-1 which is the most likely candidate for a black hole.

Most of stationary accretion disks have been calculated based on a " standard accretion disk model " (henceforce referred to SADM). In SADM it is assumed that the thickness of the accretion disk is thin compared with the radial distance from the compact star and azimuthal velocity of accreting matter is Keplerian. The SADM approximation also assumes that viscous stress which plays an important role in transport of angular momentum is proportional to total pressure. However, these stationary accretion disk models do not seem to give satisfactory results to account for peculiar

features of Cyg X-1 such as its hard X-ray tail of the spectrum and the chaotic pulses. In this respect Shapiro et al. (1976) gave a detailed " two-temperature disk model " which might be promising if radiation pressure dominated inner region of the disk was secularly unstable. On the other hand, Bisnovatyi-Kogan and Blinnikov (1977) proposed a " corona-disk model " where the accretion process would not be steady, by investigation of particle motions taking account of the radiation from the disk and gravitational field of a black hole.

Hōshi (1977), Hōshi and Shibazaki (1977), and Shibazaki (1978) showed that the structure of a stationary accretion disk around a black hole would be distinctly different from that of SADM and that the accretion disk might has non-steady characters, using a new formula for viscous stress derived by Ichimaru (1977) and taking account of the effect of the pressure gradient force in the equation of motion which has been neglected in SADM.

In this paper we investigate accretion disks around a black hole and a magnetized neutron star by means of numerical integrations of time-dependent hydrodynamical equations. Our point of view is to study the stability of the inner region of the accretion disk, rather than attempting to explain the detailed observed properties of X-ray sources, when the pressure gradient force is taken account of in the standard accretion disk model.

Time-dependent accretion disks around compact stars have been examined by Lightman (1977 a,b). From both analytic and numerical studies, he found that inner region of a disk around a black hole was secularly unstable against clumping of the gas into rings. He also argued that such an instability did not occured for a magnetized neutron star in which radiation pressure dominated inner

region of the disk did not exist. Compared with his method which is based on the SADM approximation, some improvements are made in basic equations which will be given in the next section.

In section 3 we show numerically that, if it is assumed that the viscous stress is proportional to the total pressure, the accretion disks around a black hole and a magnetized neutron star except for the latter with a low accretion rate are thermally unstable in the inner region of the disk. On the other hand the disk around the magnetized neutron star with the low accretion rate is stable on the thermal time scale and is well approximated by the SADM. In section 4 we discuss some restrictions of the used assumptions and the instabilities in the inner region of the disk.

2. Basic Equations of Disk Structure

2.1 Assumptions

We consider an axisymmetric disk structure of accreting matter and employ a cylindrical coordinate system (r, φ, z) with the z-axis chosen as the axis of rotation. Relativistic effects are neglected. This assumption will be valid for disks around magnetized neutron stars and for most of region of disks outside the last stable orbit around black holes. The disk is assumed to consist of a fully ionized hydrogen gas. Two-temperature state is not considered here , that is, the electron temperature is assumed to be equal to the ion temperature since the energy exchange time between electrons and ions is much shorter than the hydrodynamical time scale as far as the cool disk model is concerned.

It is assumed that vertical distribution of disk matter is given by a polytrope with a polytropic index 3. Z-dependences of

azimuthal and radial velocities of the disk matter are neglected although these dependences may become significant in a geometrically thick disk. In doing so, we can treat the hydrodynamical equations integrated exactly over the thickness of the disk.

As for the viscous stress $P_{r\varphi}$ we have

$$P_{r\varphi} = \eta_t \frac{r}{2} \frac{d\Omega}{dr} \quad ,$$

where η_t is the turbulent or magnetic turbulent viscosity and Ω is the angular velocity. If we assume the turbulent viscosity as $\eta_t = \rho v_t l$ and the Keplerian angular velocity for Ω, the viscous stress is reduced to the familiar α-model:

$$P_{r\varphi} = -\alpha P. \qquad (1)$$

Here ρ, v_t, and l are the density, the turbulent velocity, and the scale of the turbulent cell ($\sim$ the disk thickness), respectively. The parameter α is $\sim v_t/c_s$ and is usually believed to lie between 1 and 10^{-3} where c_s is the sound velocity. We adopt equation (1) for the viscous stress though in this paper it is not assumed that the angular velocity of the disk matter is Keplerian. Lightman (1974b) discussed that, in order to prevent the clumping instability of the thin disk model, equation (1) might be replaced by the following relation :

$$P_{r\varphi} = -\alpha P_g, \qquad (2)$$

even when the radiation pressure P_r exceeds the gas pressure P_g. This expression of the viscous stress is also used in comparison with the former. Another formula for the viscous stress was der-

ived by Ichimaru (1977). His formula is reduced to the α-model if the gas pressure dominates the radiation pressure and Keplerian motion prevails in the accretion disk, and then the parameter α becomes $\sim$ 0.8 in our case with polytropic index 3. With relation to this, the value 0.8 for the parameter α is used through later computations.

We treat only the inner region of the accretion disks around a black hole and a magnetized neutron star. For the accretion disk around the black hole, the inner edge of the disk is taken as $r_0 = 6Gm/c^2$ where G, m and c are the gravitational constant, the mass of the central star, and the velocity of light, respectively. For the magnetized neutron star, the inner edge of the disk is taken to be the Alfven radius and it is assumed that the Alfven radius remains always equal to the corotation radius. The complicated boundary layer at the Alfven surface is not considered here although it really plays a decisive role in transport of mechanical energy and angular momentum between the magnetic field and the accretion disk. To simplify the very complex situation, we treat the Alfven surface like a rigid wall. This simplification, although not quite correct, will allow a restricted application to the accretion disk around the magnetized neutron star.

2.2 Vertical Structure of Disk and Energy Loss Rate

In this subsection we refer to Hōshi (1977)'s paper. Vertical hydrostatic balance of the disk matter at a radial distance r from the center and at a vertical distance z from the disk plane is given by

$$\frac{dP}{dz} = -\frac{Gm\rho z}{r^3(1+y^2)^{3/2}} , \qquad (3)$$

where y is z/r.

Though y^2 term in equation (3) has been neglected in the usual thin disk model, it may become important for a geometrically thick disk. With the polytropic relation given by $P = K\rho^{4/3}$, the solution of equation (3) is given by

$$4K\rho^{1/3} = \frac{Gm}{r}\left(\frac{1}{\sqrt{1+y^2}} - \frac{1}{\sqrt{1+y_o^2}}\right) , \qquad (4)$$

where $y_o = z_o/r$ and z_o is the half thickness of the disk, and at the equatorial plane we have

$$4K\rho_o^{1/3} = 4\frac{P_o}{\rho_o} = \frac{Gm}{r}\frac{\sqrt{1+y_o^2}-1}{\sqrt{1+y_o^2}} , \qquad (5)$$

where P_o and ρ_o are the pressure and the density at the equatorial plane, respectively.

The equation of state is given by

$$P = \frac{1}{3}aT^4 + 2\frac{k}{m_H}\rho T , \qquad (6)$$

where T is the temperature, a the radiation density constant, k the Boltzmann constant, and m_H the hydrogen mass.

From equations (4)—(6) together with the polytropic relation, we have

$$\rho = \rho_o f(y,y_o)^3,$$

$$P = P_o f(y,y_o)^4, \qquad (7)$$

$$T = T_o f(y,y_o),$$

where

$$f(y,y_o) = \frac{\sqrt{1+y_o^2}}{\sqrt{1+y_o^2}-1}\left(\frac{1}{\sqrt{1+y^2}} - \frac{1}{\sqrt{1+y_o^2}}\right), \qquad (8)$$

and T_o is the temperature at the equatorial plane.

We define the following variables:

$$S = \text{surface density} = \int_{-Z_o}^{Z_o} \rho\, dz\ , \qquad (9)$$

$$W = \text{integrated pressure} = \int_{-Z_o}^{Z_o} P dz\ , \qquad (10)$$

$$W_{r\varphi} = \text{integrated viscous stress} = \int_{-Z_o}^{Z_o} P_{r\varphi}\, dz\ , \qquad (11)$$

$$E_r = \int_{-Z_o}^{Z_o} \varepsilon_r dz\ , \qquad (12)$$

where ε_r is the rate of radiative energy loss per unit volume of the accretion disk.

Then we have

$$S = 2\rho_o r\left(\frac{\sqrt{1+y_o^2}}{\sqrt{1+y_o^2}-1}\right)^3 g_1(y_o)\ , \qquad (13)$$

$$W = 2P_o r\left(\frac{\sqrt{1+y_o^2}}{\sqrt{1+y_o^2}-1}\right)^4 g_2(y_o)\ , \qquad (14)$$

$$W_{r\varphi} = -\alpha W \quad \text{or} \quad -\alpha W\beta\ , \qquad (15)$$

where

$$g_1(y_o)=\frac{y_o^3}{(1+y_o^2)^{3/2}}+\frac{3}{1+y_o^2}\left[\ln(y_o+\sqrt{1+y_o^2})-\sqrt{1+y_o^2}\tan^{-1}y_o\right], \quad (16)$$

$$g_2(y_o)=-\frac{5}{2}\frac{y_o}{1+y_o^2}+\frac{1}{2}\left(1+\frac{6}{1+y_o^2}\right)\tan^{-1}y_o-\frac{\ln(y_o+\sqrt{1+y_o^2})}{(1+y_o^2)^{3/2}}$$

$$-\frac{g_1(y_o)}{\sqrt{1+y_o^2}}, \quad (17)$$

and β is the ratio of the gas pressure to the total pressure and becomes independent of the z-coordinate in our case with the polytropic index 3. When $y_o \ll 1$, $g_1(y_o) \sim 2/35\ y_o^7$ and $g_2(y_o) \sim 8/315\ y_o^9$, and equations (13) and (14) coincide with equation (6) in Hōshi (1977)'s paper.

The energy loss rate E_r depends on whether the accretion disk is optically thick or thin.

In terms of the electron scattering opacity

$$\kappa_{es} = 0.4\ , \quad (18)$$

and the Rosseland mean opacity for free-free absorption

$$\kappa_{ff} = 0.64\times 10^{23}\rho\, T^{-7/2}, \quad (19)$$

the effective optical depth τ_{eff} is given by

$$\tau_{eff}=\begin{cases}(\tau_{es}\tau_{ff})^{1/2} & (\tau_{es}\geqq\tau_{ff})\\ \tau_{ff} & (\tau_{es}<\tau_{ff})\ ,\end{cases} \quad (20)$$

where

$$\tau_{es}=\int_0^{z_o}\kappa_{es}\rho dz=\kappa_{es}\rho_o r\left(\frac{\sqrt{1+y_o^2}}{\sqrt{1+y_o^2}-1}\right)^3 g_1(y_c)\ , \qquad (21)$$

$$\tau_{ff}=\int_0^{z_o}\kappa_{ff}\rho\, dz = 0.64\times 10^{23}\rho_o^{\,2}T_c^{-7/2}r\int_0^{y_o}f(y,y_o)^{5/2}dy. \qquad (22)$$

For an optically thin disk ($\tau_{eff}<1$), E_r is given by the rate of free-free emission, $\varepsilon_r=\varepsilon_o\rho T^{1/2}$, integrated over the z-coordinate,

$$E_r=2\varepsilon_o\rho_o^{\,2}T_c^{1/2}r\int_0^{y_o}f(y,y_o)^{6.5}dy. \qquad (23)$$

When $\tau_{eff}\geq 1$, the radiative energy loss is given by outward energy flux across unit area of the disk surface,

$$E_r=-2\left(\frac{4acT^3}{3\kappa\rho}\frac{dT}{dz}\right)_{surface}\ , \qquad (24)$$

where κ is the opacity. We replace approximately the opacity κ with $\bar{\kappa}$ given by the vertically averaged temperature and density. Then equation (24) becomes

$$E_r=\frac{16\ acT_o^4}{3\bar{\kappa}\rho_o z_o}\frac{y_o^2}{2(\sqrt{1+y_o^2}-1)(1+y_o^2)}=\frac{2c}{\bar{\kappa}}\frac{Gm}{r^2}\frac{y_o(1-\beta)}{(1+y_o^2)^{3/2}}. \qquad (25)$$

2.3 Hydrodynamical Equations of Disk Structure

With the difinitions (9)-(12), we can write vertically integrated hydrodynamical equations. The equations of mass, momentum, angular momentum, and energy conservations take the following form:

$$\frac{\partial}{\partial t}(rS)+\frac{\partial}{\partial r}(rSv_r)=0\ , \qquad (26)$$

$$\frac{\partial}{\partial t}(rSv_r) + \frac{\partial}{\partial r}(rSv_r^2) = -r\frac{\partial W}{\partial r} - S(\frac{Gm}{r} - v_\varphi^2), \qquad (27)$$

$$\frac{\partial}{\partial t}(r^2Sv_\varphi) + \frac{\partial}{\partial r}(r^2Sv_\varphi v_r) = \frac{\partial}{\partial r}(r^2W_{r\varphi}), \qquad (28)$$

$$\frac{\partial}{\partial t}\left[rS\left\{A\frac{W}{S} + \frac{1}{2}(v_r^2+v_\varphi^2)\right\}\right] + \frac{\partial}{\partial r}\left[rSv_r\left\{A\frac{W}{S} + \frac{1}{2}(v_r^2+v_\varphi^2)\right\} + r(Wv_r - W_{r\varphi}v_\varphi)\right]$$

$$= -rE_r - rSv_r\frac{Gm}{r^2}, \qquad (29)$$

where

$$A = 3(1-\beta) + \frac{\beta}{\gamma-1}, \qquad (30)$$

and v_r, v_φ, and γ denote the radial velocity, the azimuthal velocity, and the ratio of specific heats, respectively.

Introducing new variables

$$R=rS, \quad M=rSv_r, \quad N=rSv_\varphi, \quad \text{and} \quad E=rS\left\{A\frac{W}{S} + \frac{1}{2}(v_r^2+v_\varphi^2)\right\}, \qquad (31)$$

equations (26)– (29) are written in vector notation as

$$\frac{\partial U}{\partial t} + \frac{\partial F}{\partial r} = \Phi, \qquad (32)$$

where

$$U = \begin{pmatrix} R \\ M \\ N \\ E \end{pmatrix}, \quad F = \begin{pmatrix} M \\ \frac{M^2}{R} + rW \\ \frac{MN}{R} - rW_{r\varphi} \\ \frac{EM}{R} + r(W\frac{M}{R} - W_{r\varphi}\frac{N}{R}) \end{pmatrix}, \text{ and } \Phi = \begin{pmatrix} 0 \\ W + \frac{1}{r}(\frac{N^2}{R} - \frac{GmR}{r}) \\ W_{r\varphi} - \frac{1}{r}\frac{MN}{R} \\ -rE_r - \frac{GmM}{r^2} \end{pmatrix}. \qquad (33)$$

Equations (32) and (33) are numerically integrated by difference method under adequate initial and boundary conditions. If we obtain new values of U after time integration, the disk parameters ρ_0, T_0, β, and y_0 can be determined through equations (5),(6),(13), and (14).

The finite difference scheme used is the Lax-Wendroff-like scheme developed by Abarbanel and Goldberg (1972). The difference equations are written in an iterative form, depending on an implicit-explicit weighting factor θ and an iterative number l, and do not include the additional explicit artificial viscosity. The above authors found that the iterative method was more effective than the explicit artificial viscosity imposed on the usual Lax-Wendrof scheme, applying it to the cylindrical shock problem. Though the equations (32) and (33) have an additional angular momentum equation compared with the cylindrical shock problem, the stability and convergence of the difference equations are similarly preserved. In actual computations, we used "external" iterative scheme named by Abarbanel and Goldberg (1972) and took $\theta=0.5$ and $l=2$ from numerical tests.

2.4 Initial Conditions

Since we are interested in the existence of the stationary accretion disk, we adopt a stationary solution based on the SADM approximation as initial conditions. In SADM, Keplerian motion is assumed for the azimuthal velocity. Furthermore it is assumed that energy dissipated by viscosity is wholly radiated away through the surface of the disk. According to SADM we have (Shakura and Sunyaev 1973) :

$$-2\pi r v_r S = \dot{M} , \tag{34}$$

$$v_\varphi = \sqrt{\frac{Gm}{r}} , \tag{35}$$

$$W_{r\varphi} = -\frac{\dot{M}}{2\pi}\sqrt{\frac{Gm}{r^3}}\left(1-\sqrt{\frac{r_o}{r}}\right), \tag{36}$$

$$E_r = \frac{3}{4\pi}\frac{Gm}{r^3}\dot{M}\left(1-\sqrt{\frac{r_o}{r}}\right), \tag{37}$$

where $\dot{M}$ is the accretion rate and r_o is the inner edge of the disk. For a given accretion rate $\dot{M}$, the initial conditions and disk parameters are numerically given from the above equations together with equations (5),(6),(13)-(15),(23), and (25).

2.5 Boundary Conditions

In the difference scheme developed by Abarbanel and Goldberg (1972) which we used, it needs values of F and Φ at the inner boundary r_o. We have not at present exact knowledge of these boundary values, especially for the accretion disk around a black hole, though Stoeger (1976) gave interesting suggestions about the boundary conditions(see later discussions in section 4.1). After all, we used the inner boundary conditions of the SADM disk in which electron scattering opacity and radiation pressure dominate. The original SADM (Shakura and Sunyaev 1973) gives

$$S = 4.6\,\alpha^{-1}\dot{m}^{-1}\left(\frac{r}{r_o}\right)^{3/2}\left(1-\sqrt{\frac{r_o}{r}}\right)^{-1},$$

and

$$v_r = 7.7\times10^{10}\alpha\,\dot{m}^2\left(\frac{r}{r_o}\right)^{-5/2}\left(1-\sqrt{\frac{r_o}{r}}\right),$$

in the region of $P_r \gg P_g$ and $\kappa_e \gg \kappa_{ff}$ where $\dot{m}$ is the accretion rate in unit of the critical accretion rate.

We may specify M, M/R, N/R, E/R, W and E_r at the inner edge instead of R, N and E themselves as the boundary conditions. This enables us to exclude the complication due to the divergence of the surface density at the inner edge. Then we have the next inner boundary conditions :

$$(E_r)_o = 0, \qquad W_o = (W_{r\varphi})_o = 0,$$

$$\left(\frac{M}{R}\right)_o = (v_r)_o = 0, \qquad \left(\frac{N}{R}\right)_o = (v_\varphi)_o = \sqrt{\frac{Gm}{r_o}}, \tag{38}$$

and $$\left(\frac{E}{R}\right)_o = \left\{ A\frac{W}{S} + \frac{1}{2}(v_r^2 + v_\varphi^2) \right\}_o = \frac{1}{2}(v_\varphi)_o^2.$$

Mass flux M at the inner boundary is taken to be constantly equal to the initial value for a black hole, but zero for a magnetized neutron star.

The outer boundary was taken to be 10 r_o because of numerical reasons. At the outer boundary, accreting matter is assumed to flow inward with prescribed accretion rate and the azimuthal velocity to be always Keplerian.

3. Numerical Results

The numerical computations were performed for three cases of $\dot{m}(=\frac{\dot{M}}{\dot{M}_c}) = 10^{-2}$, 0.1, and 1.0 for a black hole with the mass of $10m_\odot$, and two cases of $\dot{m}=10^{-2}$ and 0.5 for a magnetized neutron star with the mass of 1 $m_\odot$ and the Alfven radius of 10^8cm. Here $m_\odot$ is the solar mass and $\dot{M}_c$ is the critical accretion rate corresponding to the Eddington luminosity L_E given by

$$L_E = \frac{4\pi Gmc}{\kappa_{es}}, \tag{39}$$

and

$$\dot{M}_c = \frac{2r_o L_E}{Gm}. \tag{40}$$

The computations were made based on the α-model($P_{r\varphi} = -\alpha P$) for each case of the above accretion rates and the case with $P_{r\varphi} = -\alpha P_g$ was calculated only for $\dot{m} = 0.1$ of the black hole.

3.1 Initial Disk Parameters

The initial disk parameters ρ_o, y_o, T_o, and τ_{eff} versus radius calculated are shown in figures 2-5, and 7 by solid curves. The range of the initial disk parameters ρ_o, y_o, T_o, and β in the inner region ($1 \leqq r/r_o \leqq 10$) is also listed in table 1. For both cases of the black hole and the magnetized neutron star (hereafter abbreviated as B-H and M-N-S, respectively,) with $\dot{m} = 10^{-2}$, the initial disks are gas pressure dominant, optically thick, but geometrically thin. As the initial accretion rate is higher, the disk is thicker and the ratio of radiation pressure to gas pressure increases, and contrarily the effective optical depth decreases. The central temperations T_o increase slightly with the increasing initial accretion rate and, in B-H case, the central densities ρ_o for $\dot{m} = 1.0$ are one-two orders of magnitude smaller than that for $\dot{m} = 10^{-2}$ and 0.1.

According to Shakura and Sunyaev (1973) the ratio of the disk thickness to the radius, y_o, is given by

$$y_o = 3\dot{m}\left(1-\sqrt{\frac{r_o}{r}}\right)\frac{r_o}{r}, \qquad (41)$$

in the region of $P_r \gg P_g$ and $\kappa_e \gg \kappa_{ff}$.
In order to examine the effect resulting from the y^2 term in equation (3), y_o of equation (41) is compared with ours for $\dot{m} = 0.5$ of M-N-S and 1.0 of B-H. This is shown in figures 4 and 8 by dashed curves and there the maximum difference of y_c between the original SADM and our initial disk is about factor of 2.

It is to be noted that, in our initial disk model, there was not found selfconsistent stationary solution for cases of too high accretion rate, for example, $\dot{m}$ = 1.0 of M-N-S and 10.0 of B-H. This fact suggests that the accretion disk with supercritical accretion rate differs significantly from the SADM disk.

Time integration of the hydrodynamical equations starts with the above initial conditions. In the computations a time step is taken to be shorter than the limit of the Courant conditions which now depend on the azimuthal velocities rather than the radial and sound velocities.

Time evolution of the accretion disk will be related to the drift, hydrodynamical, and thermal time scales. The drift time scale t_D is the time for gas to drift radially inward. The hydrodynamical time scale t_H is the time for sound waves to travel vertically through the disk. And an upper limit to the thermal time scale t_T is taken to be the time for a photon to random walk from $z=0$ to $z=z_o$.

The three time scales are given by

$$t_D \sim \frac{r}{v_r} \sim \alpha^{-1} \left(\frac{z_o}{r}\right)^{-2} t_H \,,$$

$$t_H \sim \frac{z_o}{c_s} \,, \quad \text{and} \quad t_T \sim \alpha^{-1} t_H \,, \tag{42}$$

as long as the disk is thin (Lightman 1974 a). Therefore we have $t_H \sim t_T \ll t_D$ since $\alpha \sim 0.8$ in our case.

From the initial disk the hydrodynamical time scale is given by , at $r=3r_c$,

$$t_H \text{ in B-H} \sim \begin{cases} 1.3 \times 10^{-2} \text{ sec} & \text{for } \dot{m} = 10^{-2} \\ 3 \times 10^{-2} \text{ sec} & \text{for } \dot{m} = 0.1, \end{cases}$$

and

$$t_H \text{ in M-N-S} \sim \begin{cases} 1.5 \text{ sec} & \text{for } \dot{m} = 10^{-2} \\ 4 \text{ sec} & \text{for } \dot{m} = 0.5 \end{cases} .$$

Based on these time scales, we deduce the initial effect of the pressure gradient force on mass flux. The variance ΔM of mass flux M due to the pressure gradient force on the thermal time scale t_T will be roughly estimated to be $-r(\partial W/\partial r)t_T$ since in the initial disk the gravitational force balances the centrifugal force. Then we have

$$\frac{\Delta M}{M} \sim \frac{(2\pi r \frac{\partial W}{\partial r} t_T)}{\dot{M}} \quad \text{for initial disk}$$

$$= \frac{2}{\alpha}\sqrt{\frac{Gm}{r_o^3}} \left(\frac{r}{r_o}\right)^{-3/2} \left(\sqrt{\frac{r_o}{r}} - \frac{3}{4}\right) t_T . \qquad (43)$$

If $|\Delta M/M| \ll 1$, the effect of the pressure gradient force on the SADM disk is negligible. Figure 1 gives the value of $\Delta M/M$ versus radius for the black hole which is almost same as that for the magnetized neutron star considered here. The figure shows that the pressure gradient force acts strongly near the inner edge of the initial disk and can influences on wider region for more luminous accretion disk.

3.2 Time Evolution of Disk around a Black Hole

Firstly let us mention the numerical results in the case of the α-model. We find in this case that the accretion disk around the black hole with any accretion rate ($\dot{m} = 10^{-2} \sim 1.0$) is thermally unstable and a strong instability developes near the inner edge of the disk. This is caused by the effect of the pressure gradient force and its coupling with the angular momentum through the viscous stress.

As the time integration proceeds, the disk deviates gradually from the SADM disk and evolves toward radiation pressure dominant, optically thin, but geometrically thick state. With further time integrations, the disk thickness y_o grows up to be comparable to unity and then an instability developes near the inner edge of the disk. Finally the instability grows abruptly and the computations can not proceed any further. The instability developes on time scales of 5×10^{-2}, 4×10^{-2}, and 2×10^{-2} sec for cases of $\dot{m} = 10^{-2}$, 0.1, and 1.0, respectively. These time scales indicate that the instability is developed by the thermal time scale in the previous subsection.

The disk parameters versus radius at the phase before the strong instability are given in figures 2-4 by dotts. The disk with the higher accretion rate suffers stronger variance of the disk parameters over the extended region on the shorter time scale. At the final stage the thickness of the disk becomes greater by several factors to more than one order of magnitude than the initial thickness and the central densities are lowered by the same extent. The case of the critical accretion rate shows typically an oscillatory behaviour of the disk parameters. The oscillation developes soon into a strong instability which accompanies a large peak of y_o and a sharp decrement of ρ_o near $r/r_o = 1.3$. To see specifically the feature of the instability at the final stage, we plot the disk thickness z_o versus radius for $\dot{m} = 0.1$ and 1.0 in figures 6a and 6b.

Figures 7a and 7b show v_φ/v_K versus radius in the course of evolution of the disk for $\dot{m} = 0.1$ and 1.0 where v_K is the Keplerian velocity. The figures show considerably variable departures of the azimuthal velocities from the Keplerian velocities.

In the initial disk with $\dot{m} = 10^{-2}$ the gas pressure and electron scattering opacity are dominant. The SADM disk in this situation gives

$$S = 1.7 \times 10^{5} \alpha^{-4/5} \dot{m}^{3/5} \left(\frac{m}{m_{\odot}}\right)^{1/5} \left(\frac{r}{r_{\circ}}\right)^{-3/5} \left(1-\sqrt{\frac{r_{\circ}}{r}}\right)^{3/5},$$

and

$$v_r = 2 \times 10^{6} \alpha^{4/5} \dot{m}^{2/5} \left(\frac{m}{m_{\odot}}\right)^{-1/5} \left(\frac{r}{r_{\circ}}\right)^{-2/5} \left(1-\sqrt{\frac{r_{\circ}}{r}}\right)^{-3/5},$$

accordingly $W/S \to 0$ and $v_r \to \infty$ as $r \longrightarrow r_{\circ}$.
However we used the boundary condition of $v_r = 0$ at $r = r_{\circ}$.
To see whether the result for $\dot{m} = 10^{-2}$ might be attributed to the inner boundary condition or not, some cases with the inner boundary condition of non-zero v_r $(0 > v_r \geq -c/3)$ were examined. As the result, the disk parameters showed same behaviour as the previous one. Therefore it is concluded that such difference of the boundary condition of v_r does not influence largely on the result.
The result for the modified boundary condition of $v_r = -c/3$ is given in figure 2 by crosses.

In the outer part of our disk, there found no variance of the disk parameters on the thermal time scale. But the disk parameters may be variable on the drift time scale which is much longer than the thermal time scale.

The above numerical results are interpreted as follows.
The initial SADM disk in which the pressure gradient force has been neglected has possitive pressure gradient below a radius r_1 ($\sim 1.8\ r_{\circ}$) and negative pressure gradient above the radius r_1. In the former region ($r < r_1$) the absolute value of the pressure gradient is larger in inner part of the region. After time integration starts, the pressure gradient force operates inward in the region and mass flux there increases more in the inner part of the region since $\partial M/\partial t$

$\sim -r(\partial W/\partial r)$ in the initial stage. This results in lower surface density and larger integrated pressure since initially $\Delta E \propto \Delta W$. Also in the latter region ($r > r_1$), same process works up to $r \sim 3.2\ r_o$ at which initial pressure gradient has its minimum value (see figure 1). The resultant variance of the integrated pressure gradient leads to a variance of angular momentum through viscous stress $W_{r\varphi} = -\alpha W$ and causes a small departure of the azimuthal velocity from the Keplerian velocity. Even if the departure of the azimuthal velocity is at first small, it influences on mass flux and again integrated pressure so long as $|(v_\varphi/v_K)^2 - 1| \times$ (centrifugal force) $\sim$ (pressure gradient force). Thus, the coupling of the pressure gradient force with the angular momentum through the viscous stress will be gradually amplified. If $\alpha \ll 1$ or $W_{r\varphi} = -\alpha W \beta$ and $\beta \ll 1$, the effect of the coupling may be negligibly small because the contribution of the viscous stress to it is small. The variable feature of angular momentum transport which is caused by the above process influences strongly on the energy generation rate in the disk and leads to thermal unbalance. If the disk is thermally unstable, the resultant fluctuations of the disk parameters develope to a strong instability on the thermal time scale.

Next let us refer to time evolution of the disk with $\dot{m} = 0.1$ when the viscous stress of $P_{r\varphi} = -\alpha P_g$ is used. The initial disk for this case is not largely different from that of $\dot{m} = 0.1$ in the α-model, except for ρ_o which is higher by several factors than that in the α-model. However, the time evolution of the disk differs from the case of the α-model. The disk parameters do not change drastically on the thermal time scale and there occurs no instability at the inner region of the disk. Moreover, the disk seems to approach a steady state. The stable behaviour of the disk is also

explainable in terms of the previous interpretation since β is small ($\lesssim 0.04$) in the inner part of the disk. The existence of such stable accretion disk has ever been discussed by Lightman and Eardley (1974) and Lightman (1974 b) in terms of the secular instability. The above result ascertains, in a sense, that the instabilities occured in the α-model were never induced by a numerical instability. The disk parameters versus radius at the phase of 6.8×10^{-2}sec are shown in figure 5.

The case of $\dot{m} = 0.1$ and $m = 10\ m_{\odot}$ stands for the approximate accretion rate and mass of Cyg X-1. The observations of Cyg X-1 show chaotic pulses on time scales from tens of seconds to ~ 50 milliseconds and hard X-rays which are currently explainable by Comptonization process at a high temperature ($\sim 10^9$K) inner region of the accretion disk. Accordingly the stable and cool disk for $\dot{m} = 0.1$ of B-H is unfavourable because it can not account for such observations.

3.3 Time Evolution of Disk around a Magnetized Neutron Star

The initial disk around the magnetized neutron star with $m = 10^{-2}$ is wholly dominant in gas pressure and optically thick and is similar to the disk around the black hole with the same accretion rate. The time evolution of the disk was examined to the time of 14 sec which is much longer than the thermal time scale but is still short compared with the drift time scale. The disk does not deviate largely from its initial state and azimuthal velocity is almost Keplerian. The difference between the black hole and the magnetized neutron star is ascribed to the different inner boundary condition. The inner boundary of the disk around the magnetized neutron star was treated as a rigid wall, while, in the black hole

case, a constant mass flux was shed inward at the inner boundary. Therefore, in the vicinity of the inner edge of the disk, the effect of the pressure gradient force in the case of the neutron star does not work in the same way as the black hole.

In the case of $\dot{m}=0.5$ the initial disk is dominant in radiation pressure and optically thick. We found that the disk was unstable and a strong instability developed on the thermal time scale. The difference between the evolutions of the disks with $\dot{m}=10^{-2}$ and 0.5 is attributed to the different degree of coupling of the pressure gradient force with the angular momentum. We may estimate the variance of angular momentum rN through the viscous stress on a time step Δt to be $\propto (\partial W_{r\varphi}/\partial r)\Delta t$ initially. Then the degree of the effect of the pressure gradient force on the angular momentum, $(\Delta N/N)$, is expressed to be $\propto (\partial W_{r\varphi}/\partial r)\Delta t/N$ by the analogy of the effect of the pressure gradient force on mass flux. The initial disks show that $(\partial W_{r\varphi}/\partial r)/N$ for $\dot{m}=0.5$ is one order of magnitude larger than that for $\dot{m}=10^{-2}$ although $(\partial W/\partial r)/M$ is independent on the accretion rate. Therefore it is expected that the coupling of the pressure gradient force with the angular momentum through the viscous stress becomes much strong compared with the case of the low accretion rate.

The disk parameters versus radius for $\dot{m}=0.5$ at the phase of 2.5 sec are given in figure 8 by dotts, and the disk thickness z_o versus radius at the final phase is shown in figure 6c. Figure 7c shows v_φ/v_K versus radius at two phases near the final stage.

3.4 Summary of Results

The numerical results are summarized as follows :

(1) When the usual α-model for viscous stress is used, accretion disks around a black hole and a magnetized neutron star except for the latter with a low accretion rate are thermally unstable. The disks deviate considerably from the standard accretion disk model near the inner edge of the disk and evolve toward the radiation pressure dominant, optically thin, but geometrically thick state, and a strong instability developes near the inner edge. On the other hand, an accretion disk around the magnetized neutron star with the low accretion rate is stable on the thermal time scale and the disk structure is well approximated by the standard disk model. These results are due to the effect of the pressure gradient force and its coupling with angular momentum through the viscous stress. The pressure gradient force and its coupling with the angular momentum become more effective for more luminous accretion disk and inner part of the inner region of the disk.

(2) When we assume $P_{r\varphi} = -\alpha P_g$ in the case of $P_r \gg P_g$, the disk around the black hole is stable and is well approximated by the SADM disk even in the inner region of the disk. This is due to the coupling of the pressure gradient force with the angular momentum being uneffective since the effect of the viscous stress is small. But the stable and cool disk model is unfavourable to account for the observations of Cyg X-1.

4. Discussion

4.1 Restriction on Assumptions

The numerical results are based on several assumptions and approximations. The most uncertain assumption is that of viscous stress which is connected with existence of turbulent and magnetic fields in a differentially rotating medium, and our results depend strongly on the viscous stress. The α-model for the viscous stress has been mostly used in spite of its uncertain. Even if the α-model is qualitatively reasonable, the parameter α may depend both on radius and the z-coordinate. In such situation the results may be altered. In this respect we must await a better theoretical and experimental study of turbulent mechanism and chaotic magnetic fields in astrophysical conditions. Hereafter, however, we will discuss on the numerical results assuming that the α-model is justifiable.

We have assumed in the basic equations that azimuthal and radial velocities are independent on the z-coordinate. The assumption may be invalid in the geometrically thick disk. In the geometrically thick disk, it will be reasonable to consider that the accreting matter of the disk rotates differentially and meridional motions are induced. In such thick and luminous accretion disk, vertical flow may play an important role and convection in vertical energy transport which has been neglected in our treatment may be replaced by radiative transport process. These factors which invalidiate the assumption may act on the disk structure particularly at the final stage of our computations where the disk thickness y_o is comparable to unity. However, we believe that the general features of time evolution toward the final stages are still reliable.

We have not taken account of the effect of Comptonization in energy loss rate. The effect becomes significant if electron scattering opacity is dominant and electron temperatures are too high. In the disk considered here, electron scattering opacity dominates everywhere but the disk temperatures are relatively low ($10^6 \sim 10^7$K) to produce a strong enhancement of the radiative energy loss by Compton cooling. Accordingly the results may not be largely altered by the effect of Comptonization.

As to the instabilities found near the inner edge, one may consider that the instabilities might be removed by adopting other appropriate inner boundary conditions instead of that of the SADM disk. The SADM assumes that the viscous stress at the inner edge is zero and radiation emitted from $r < r_o$ is negligible when the compact star is a black hole. In regard to this, Stoeger(1976) demonstrated that the condition of $W_{r\varphi}=0$ at $r=r_o$ is physically unrealistic since it leads to too abrupt variations of the density and the radial velocity near the inner edge and that one should loosen the condition to more realistic condition, for example, $d^2W_{r\varphi}/dr^2=0$ at $r=r_o$. Such modification of the boundary conditions may result in non-zero of W/S and E_r in equation (38) and non-Keplerian velocity of v_φ at the boundary. We did not investigate the effects of the modified conditions and so can not exclude the possibility that these may remove the instabilities found in this paper.

4.2 Comparison with Other Results

The effect of pressure gradient force on the structure of the stationary accretion disk around a black hole has been studied by Hōshi and Shibazaki (1977) and Shibazaki (1978) who solved numerically the full set of steady state equations using a new formula

of viscous stress derived by Ichimaru (1977). They found that none of solutions converges to the SADM solution except only for the extremely limited range of the outer boundary condition and could not obtain a complete structure of the stationary and optically thick disk extending into the vicinity of the black hole. This follows from the fact that the pressure gradient force couples strongly with the viscous stress and alters the structure of the disk completely even for a thin accretion disk. As the results they proposed the two possibilities :

(a) An accretion disk can adjust the outer boundary condition so as to bring a steady state.

(b) The accretion disk has non-steady characters.

Our results show that the possibility (b) may be established in the inner region of the disk around the black hole with moderate or high accretion rate. In our computations only the inner region of the disk was treated and there found no large variance of the region. But it does not conclusively mean that the outer region settles in a SADM state. As to the question and the possibility (a), it needs for us to examine time-dependent structure of the outer region of the disk over the drift time scale.

The thermal and secular instabilities of the accretion disk around a black hole were studied by several authors (Lightman and Eardley 1974, Lightman 1974b, Shibazaki and Hōshi 1975, Shakura and Sunyaev 1976, and Pringle 1976). In the stability analyses it has been assumed that matter in the disk is thoroughly in Keplerian motion since the pressure gradient force is usually small compared with the centrifugal and gravitational forces. Our results show that, in addition to their stability analyses, the pressure gradient force plays also an important role in the

stability problem of the accretion disk, especially near the inner edge of the disk even if the disk is thin.

For example, as for the secular instability, they consider an evolution equation of surface density S given

$$\frac{\partial S}{\partial t} = \frac{1}{r\partial r}\left\{ \left(\frac{drv_\varphi}{dr}\right)^{-1}\frac{\partial}{\partial r}(r^2 W_{r\varphi})\right\} . \qquad (44)$$

The integrated viscous stress is written in a form of $W_{r\varphi} \propto S^n$ from the initial stationary disk. The stability criterion is that the disk is secularly unstable for negative n when $(drv_\varphi/dr)^{-1}$ in equation (44) is possitive, for example, v_φ is equal to the Keplerian velocity.

The growth time t_{inst} of the perturbation is given by

$$t_{inst} = \frac{1}{8\pi^2 |n|}\left(\frac{\lambda}{r}\right)^2 t_D \gtrsim \frac{t_T}{8\pi^2 |n|} , \qquad (45)$$

where λ is the wave length of the perturbation. The equation (45) is applicable for perturbations of $r \gg \lambda \gtrsim z_0$.

Our initial disks give

$$n = \begin{cases} -1 & \text{for } P_r \gg P_g \text{ and } \tau_{eff} > 1, \\ 5/3 & \text{for } P_g \gg P_r \text{ and } \tau_{eff} > 1, \\ 41/23 & \text{for } P_r \gg P_g \text{ and } \tau_{eff} < 1 . \end{cases}$$

Accordingly the initial disks will be unstable for the cases of $\dot{m} = 0.1$ of B-H and $\dot{m} = 0.5$ of M-N-S but stable for the other cases. The numerical results for $\dot{m} = 10^{-2}$ and 1.0 of B-H contradict with the above criterion. However, we notice that the pressure gradient force is not taken into account in the stability analysis.

As we mentioned before, the effect of the pressure gradient force and its coupling with angular momentum through viscous stress alter significantly the disk structure near the inner edge of the disk and result in strong fluctuations of the azimuthal velocities. The variable transport of the angular momentum along the radial direction influences strongly on the energy equation. Therefore the above stability criterion can not be applicable to such cases. The actual numerical results show that the disks become unstable even for the cases of $\dot{m} = 10^{-2}$ and 1.0 of B-H.

The unstable character of the inner region of the accretion disk investigated in this paper is advantageous to explain the observed variability of radiation from Cyg X-1. Following the unstable configuration of the disk, we consider that the thermal instability occurred in the inner region may drive the cool disk to a hot two-temperature state as was demonstrated by Shapiro et al.(1976) or that a high temperature corona analogous to the solar corona (Bisnovatyi-Kogan and Blinnikov 1977, Liang 1977, and Liang and Price 1977) may be formed in the inner region of the disk if convection prevails in vertical energy transport. Further works in that direction should be developed in the future.

The author is grateful to Professors S. Ueno and R. Hōshi for their kind and critical reading of the manuscript. He also thanks Professor S. Sakashita and Drs. N. Kaneko and S. Ikeuchi for their valuable discussions during this work. Numerical computations were carried out on a FACOM 230-75 at the Computer Center of Hokkaido University.

References

Abarbanel, S., and Goldberg, M. 1972, Journal of Computational Physics, 10, 1.

Bisnovatyi-Kogan, G.S., and Blinnikov, S.I. 1977, Astron. Astrphys., 59, 111.

Hōshi, R. 1977, Prog. Theor. Phys., Kyoto, 58, 1191.

Hōshi, R., and Shibazaki, N. 1977, Prog. Theor. Phys., Kyoto, 58, 1759.

Ichimaru, S. 1977, Astrophys. J., 214, 840.

Liang, E.P.T. 1977, Astrophys. J. Letters, 211, 67.

Liang, E.P.T., and Price, R.H. 1977, Astrophys. J., 218, 247.

Lightman, A.P. 1974a, Astrophys. J., 194, 419.

Lightman, A.P. 1974b, Astrophys. J., 194, 429.

Lightman, A.P., and Eardley, D.M. 1974, Astrophys. J. Letters, 187, 1.

Novikov, I.D., and Thorne, K.S. 1973, in Black Hole, ed. C. DeWitt, and B. DeWitt (Gordon and Breach, New York).

Pringle, J.E. 1976, Monthly Notices Roy. Astron. Soc., 177, 65.

Pringle, J.E., and Rees, M.J. 1972, Astron. Astrophys., 21, 1.

Shakura, N.I., and Sunyaev, R.A. 1973, Astron. Astrophys., 24, 337.

Shakura, N.I., and Sunyaev, R.A. 1976, Monthly Notices Roy. Astron. Soc., 175, 613.

Shapiro, S.L., Lightman, A.P., and Eardley, D.M. 1976, Astrophys. J., 204, 187.

Shibazaki, N. 1978, Prog. Theor. Phys., Kyoto, 60, 985.

Shibazaki, N., and Hōshi, R. 1975, Prog. Theor. Phys., Kyoto, 54, 706.

Stoeger, W.R. 1976, Astron. Astrophys., 53, 267.

Table 1. The range of initial disk parameters in the inner region ($1 < r/r_o \leq 10$) of the accretion disks around the compact stars when the α-model is used.

	Black hole			Magnetized neutron star	
$\dot{M}/\dot{M}_c$	10^{-2}	0.1	1.0	10^{-2}	0.5
ρ_o (g/cm^3)	2.2×10^{-2}–1.7×10^{-3}	2.6×10^{-2}–1.7×10^{-3}	3.5×10^{-4}–1.2×10^{-5}	3.7×10^{-4}–2.5×10^{-5}	7.2×10^{-4}–4.9×10^{-5}
z_o/r	7×10^{-3}–2×10^{-2}	1.4×10^{-2}–4.9×10^{-2}	0.14–0.41	2.9×10^{-2}–6.5×10^{-2}	7.8×10^{-2}–0.28
T_o (K)	8.0×10^{6}–2.5×10^{6}	1.4×10^{7}–5.5×10^{6}	1.7×10^{7}–6.1×10^{6}	1.3×10^{6}–4.0×10^{5}	4.2×10^{6}–1.6×10^{6}
β	0.9–0.7	0.5–0.1	7.1×10^{-3}–3.6×10^{-3}	0.97–0.91	0.57–0.10

Captions

Fig.1 $\left(\frac{2\pi r \frac{\partial W}{\partial r} t_T}{\dot{M}}\right)$ for initial disk versus radius for the black hole with $\dot{M}/\dot{M}_c=10^{-2}$ and 0.1. It shows the degree of initial effect of pressure gradient force on mass flux.

Fig.2 Disk parameters ρ_o, z_o/r, T_o, and τ_{eff} of the black hole with $\dot{M}/\dot{M}_c=10^{-2}$ at the initial stage (solid lines) and the stage after 4.5×10^{-2} sec (dotts). Crosses denote the values when an inner boundary condition of $v_r=-c/3$ is used.

Fig.3 Disk parameters ρ_o, z_o/r, T_c, and τ_{eff} of the black hole with $\dot{M}/\dot{M}_c=0.1$ at the initial stage (solid lines) and the stage after 3.86×10^{-2}sec (dotts).

Fig.4 Disk parameters ρ_o, z_c/r, T_o, and τ_{eff} of the black hole with $\dot{M}/\dot{M}_c=1.0$ at the initial stage (solid lines) and the stage after 1.36×10^{-2} sec (dotts). Dashed lines in z_o/r diagram denote the original SADM.

Fig.5 Disk parameters ρ_o, z_o/r, T_o, and τ_{eff} of the black hole with $\dot{M}/\dot{M}_c=0.1$ at the initial stage (solid lines) and the stage after 6.75×10^{-2} sec (dotts) when the viscous stress of $P_{r\varphi} = -\alpha P_g$ is used.

Fig.6 Disk thickness z_o versus radius at the final stages for the black hole with $\dot{M}/\dot{M}_c=0.1$(a) and 1.0(b) and magnetized neutron star with $\dot{M}/\dot{M}_c=0.5$(c). Dashed lines denote the SADM.

Fig.7 Ratio of azimuthal velocity to Keplerian velocity versus radius in the course of evolution of the disks around the black hole (a,b) and magnetized neutron star (c).

Fig.8 Disk parameters ρ_o, z_o/r, T_o, and τ_{eff} of the magnetized neutron star with $\dot{M}/\dot{M}_c=0.5$ at the initial stage (solid lines) and the stage after 2.48 sec (dotts). Dashed lines in z_o/r diagram denote the original SADM.

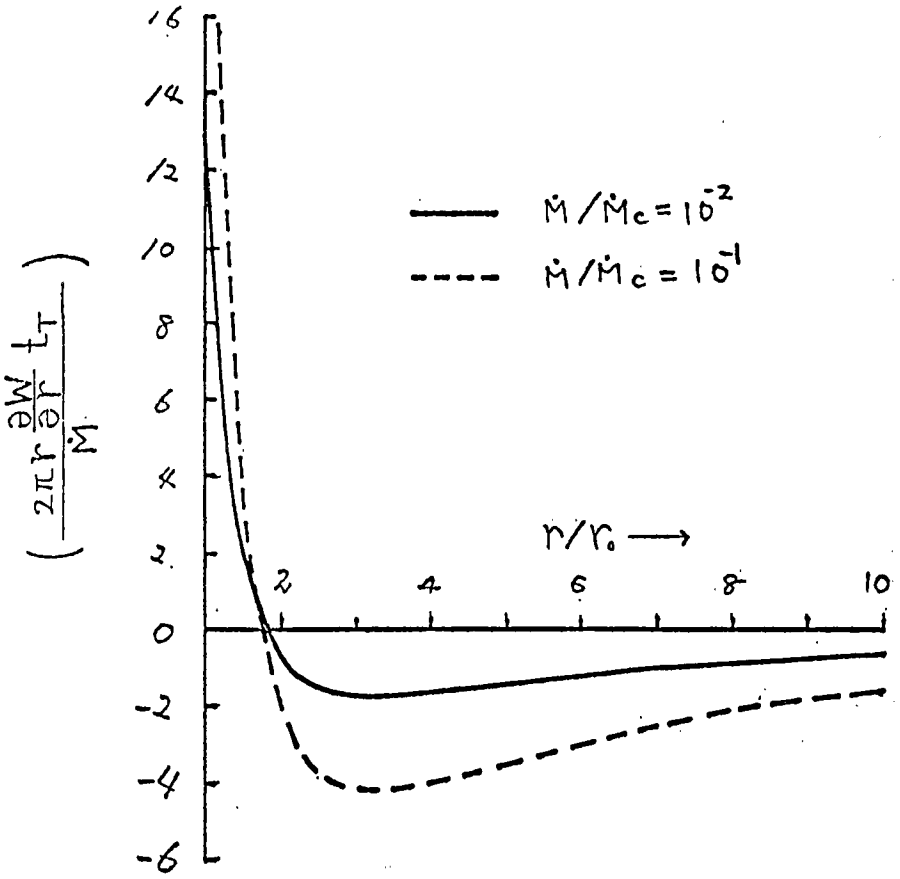
16
14
12
10
8
6
4
2
0
-2
-4
-6
$\left(\frac{2\pi r \frac{\partial W}{\partial r} t_T}{\dot{M}}\right)$
$\dot{M}/\dot{M}_c = 10^{-2}$
$\dot{M}/\dot{M}_c = 10^{-1}$
$r/r_0 \longrightarrow$
2
4
6
8
10

Fig. 1

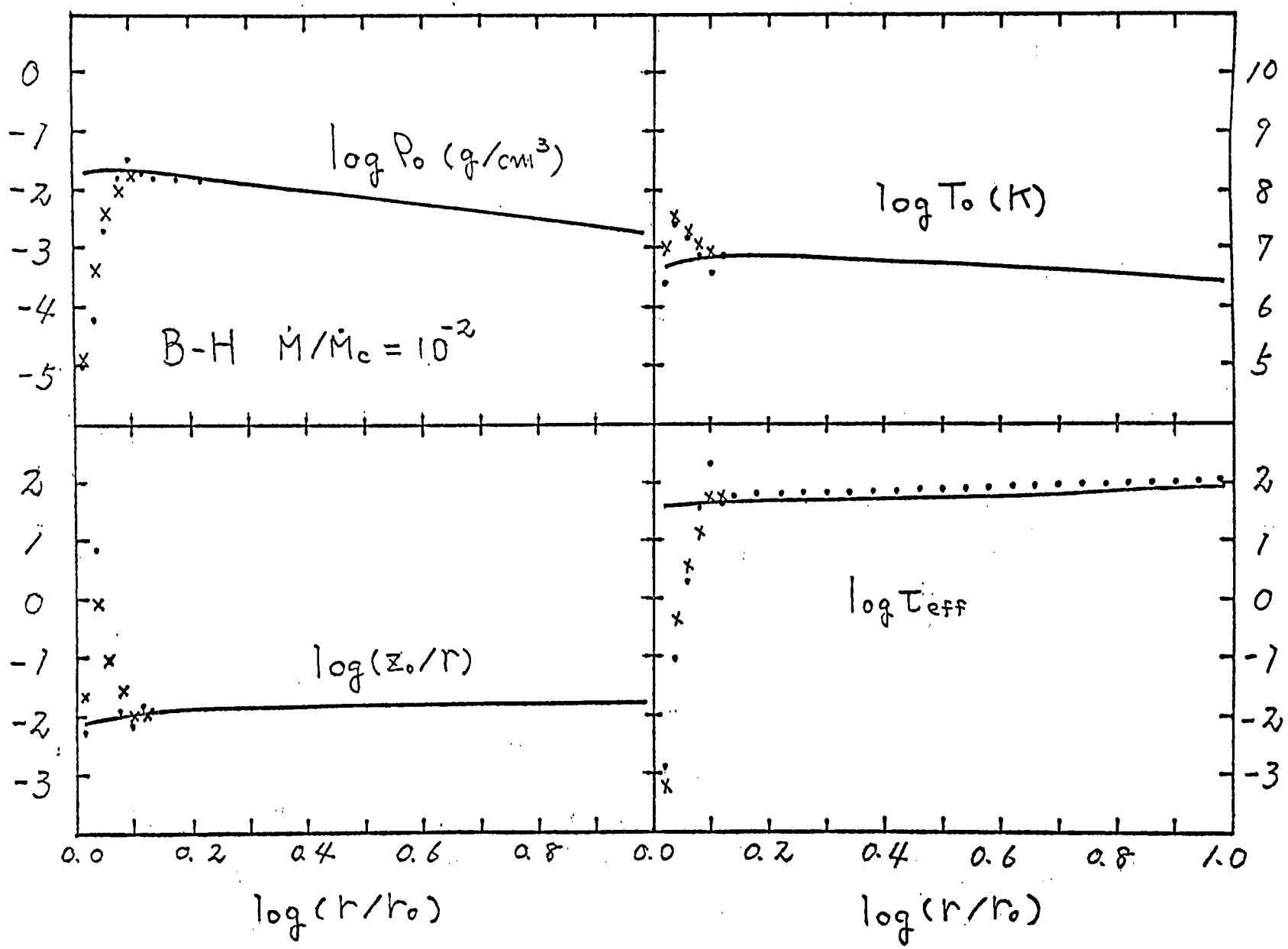

Fig. 2

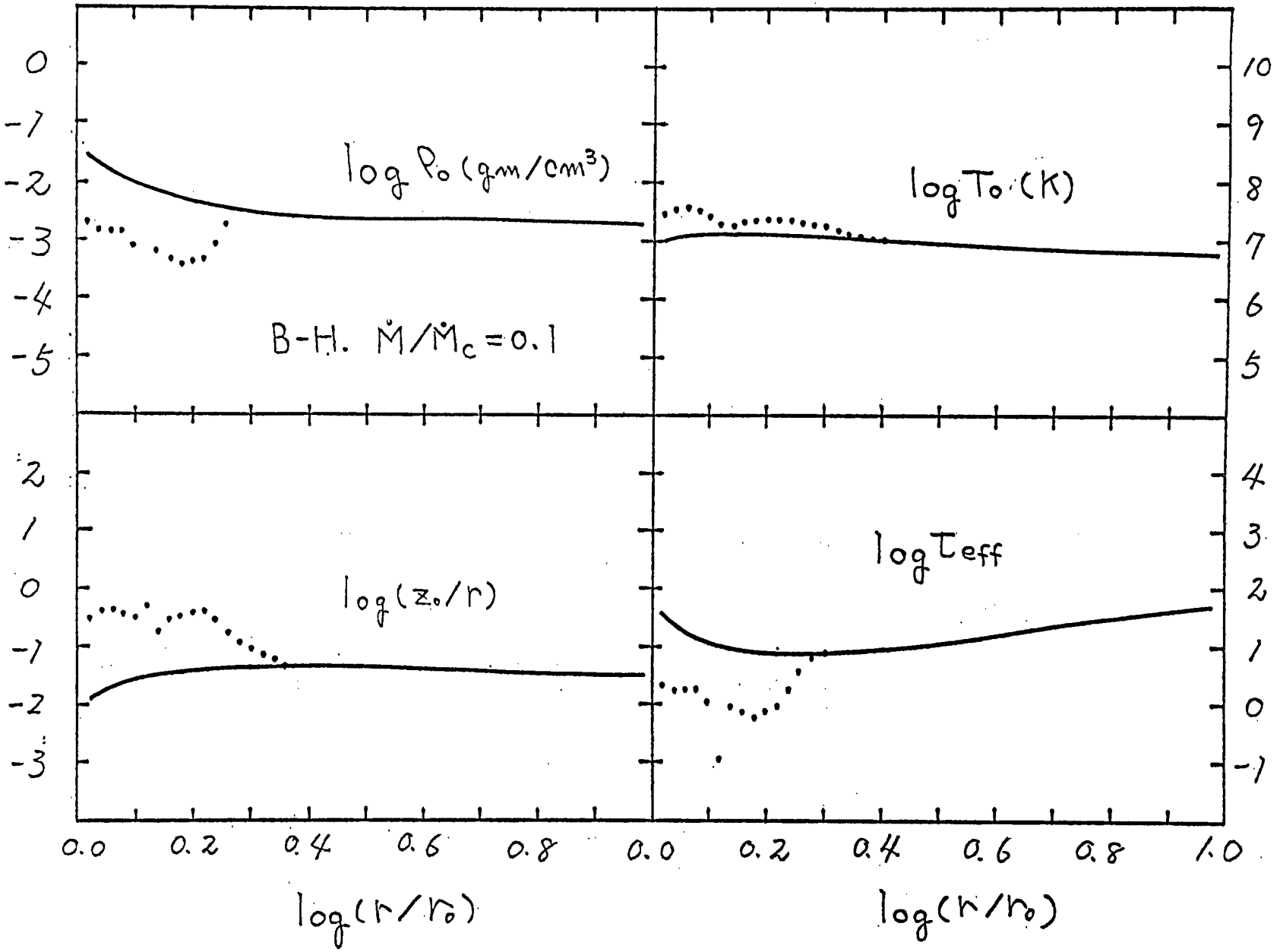
log ρ_o (gm/cm^3)
log T_o (K)
B-H. $\dot{M}/\dot{M}_c = 0.1$
log (z_o/r)
log T_{eff}
log(r/r_o)
log(r/r_o)

Fig 3

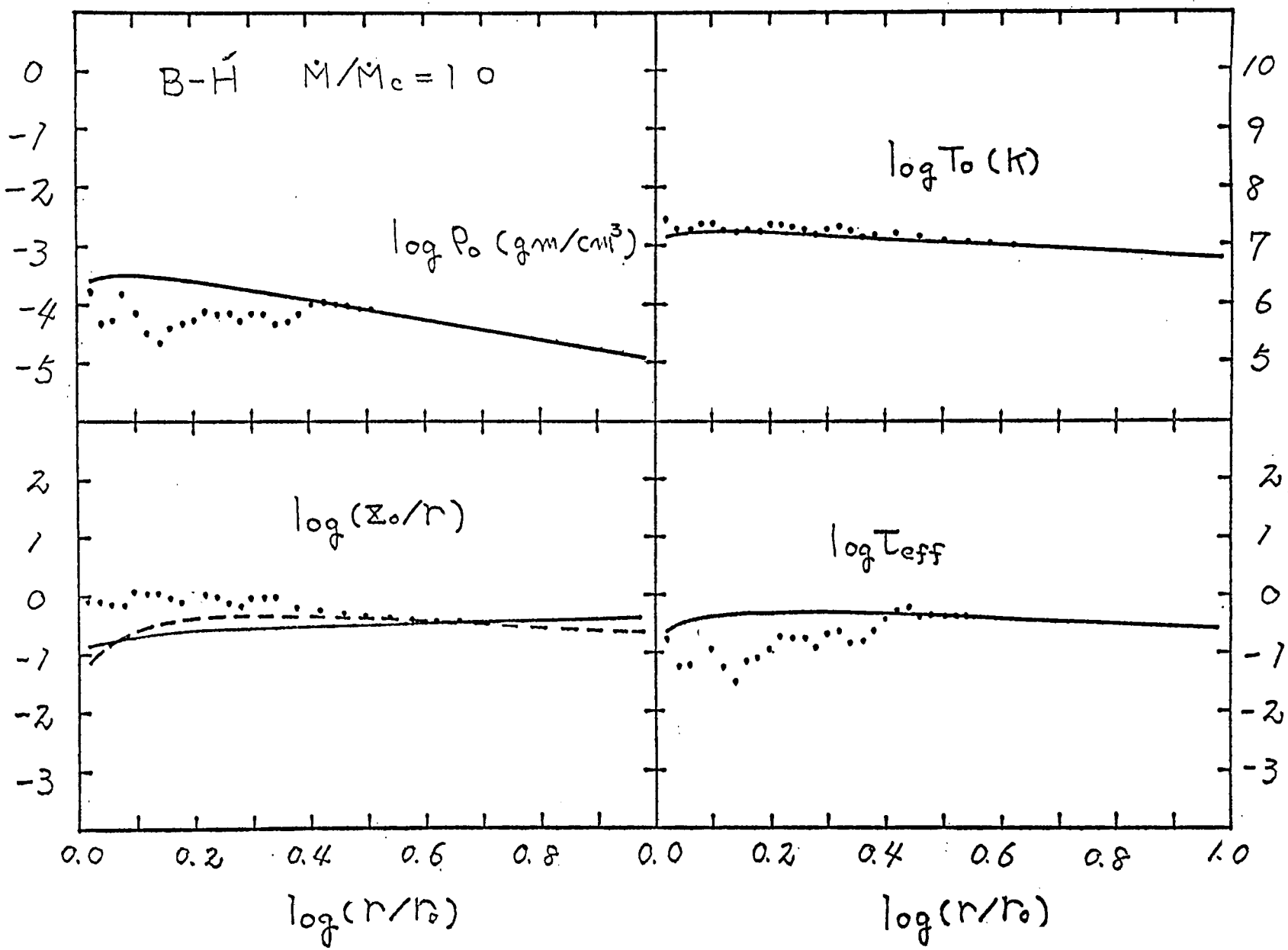
B-H Ṁ/Ṁc = 1 0
log P0 (gm/cm³)
log T0 (K)
log (z0/r)
log Teff
log (r/r0)
log (r/r0)
0
-1
-2
-3
-4
-5
10
9
8
7
6
5
2
1
0
-1
-2
-3
0.0
0.2
0.4
0.6
0.8
1.0

Fig. 4

Fig. 5

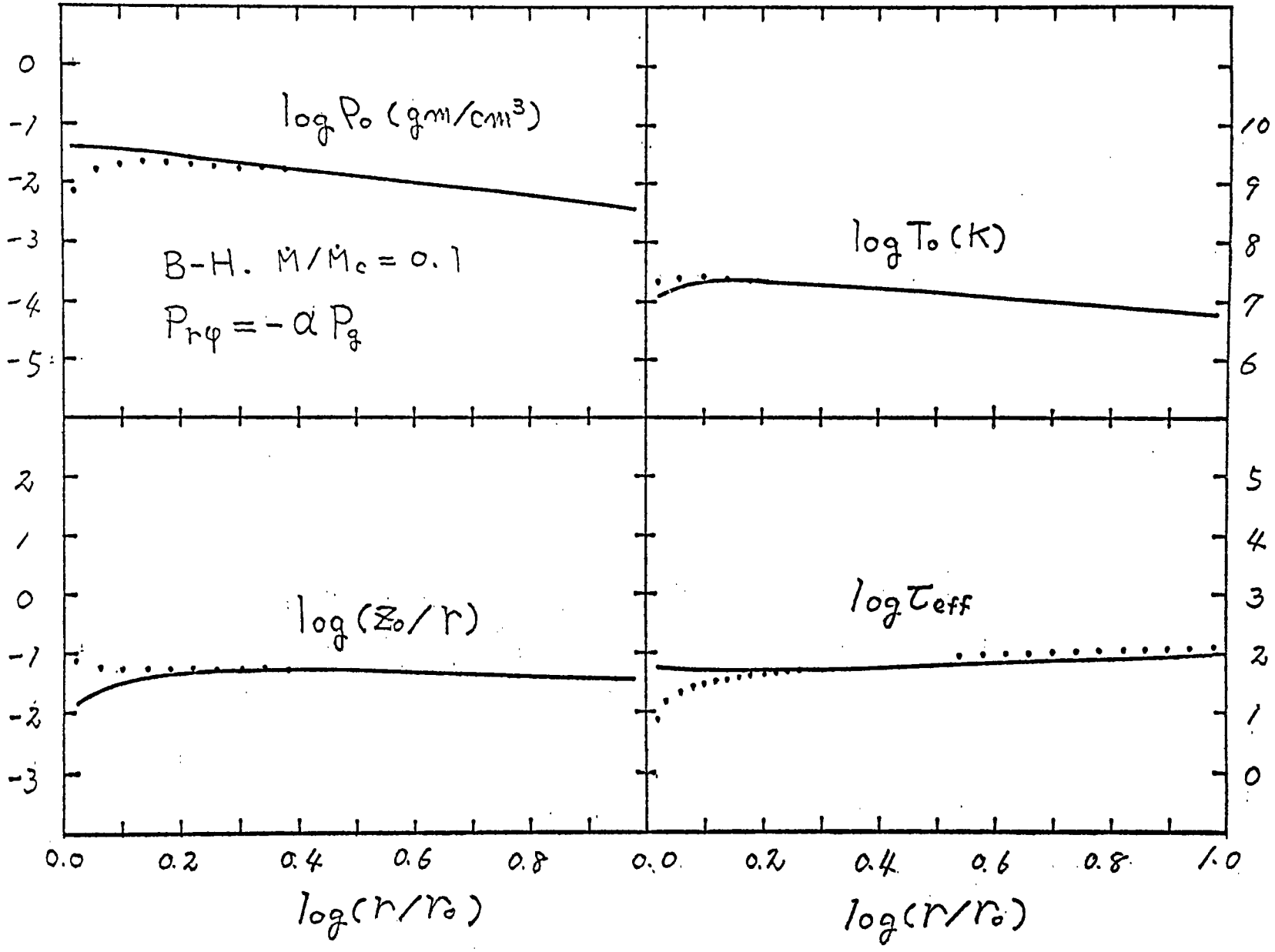
log P₀ (gm/cm³)
B-H. Ṁ/Ṁc = 0.1
Prφ = −α Pg
log T₀ (K)
log (z₀/r)
log τeff
log (r/r₀)
log (r/r₀)
0
-1
-2
-3
-4
-5
10
9
8
7
6
2
1
0
-1
-2
-3
5
4
3
2
1
0
0.0
0.2
0.4
0.6
0.8
1.0

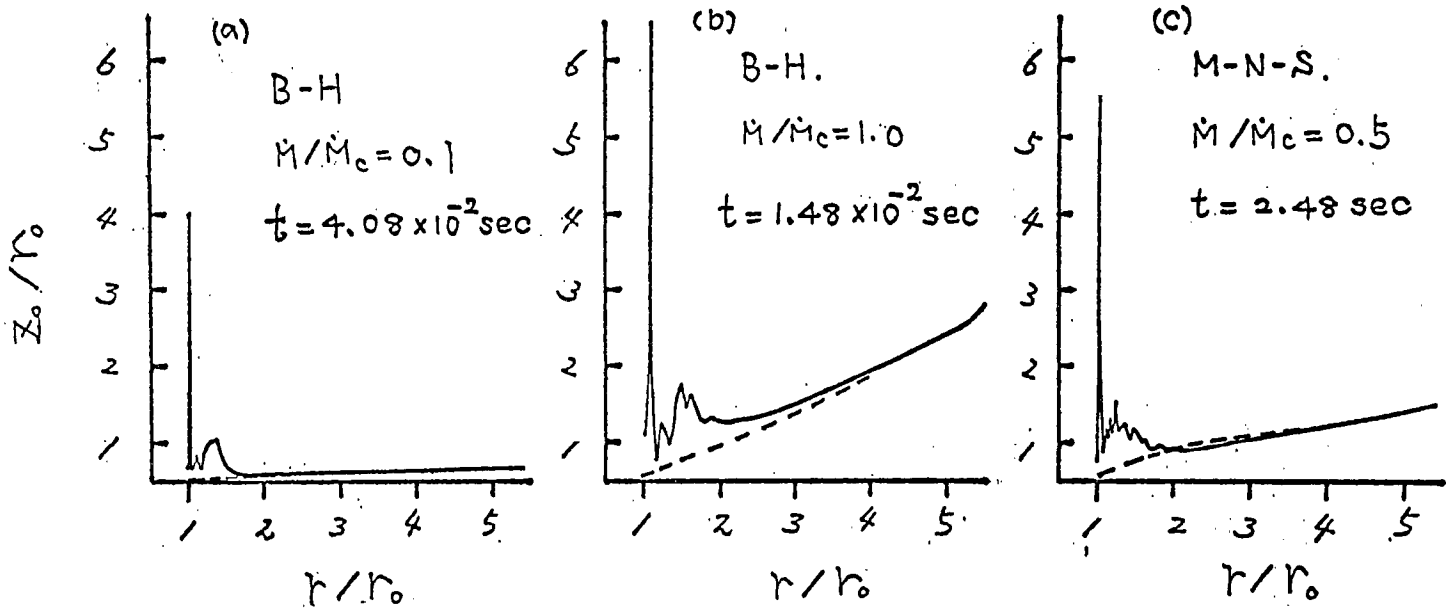
(a)
B-H
Ṁ/Ṁc = 0.1
t = 4.08 x 10⁻² sec
(b)
B-H.
Ṁ/Ṁc = 1.0
t = 1.48 x 10⁻² sec
(c)
M-N-S.
Ṁ/Ṁc = 0.5
t = 2.48 sec
Z₀/r₀
r/r₀
r/r₀
r/r₀

Fig 6

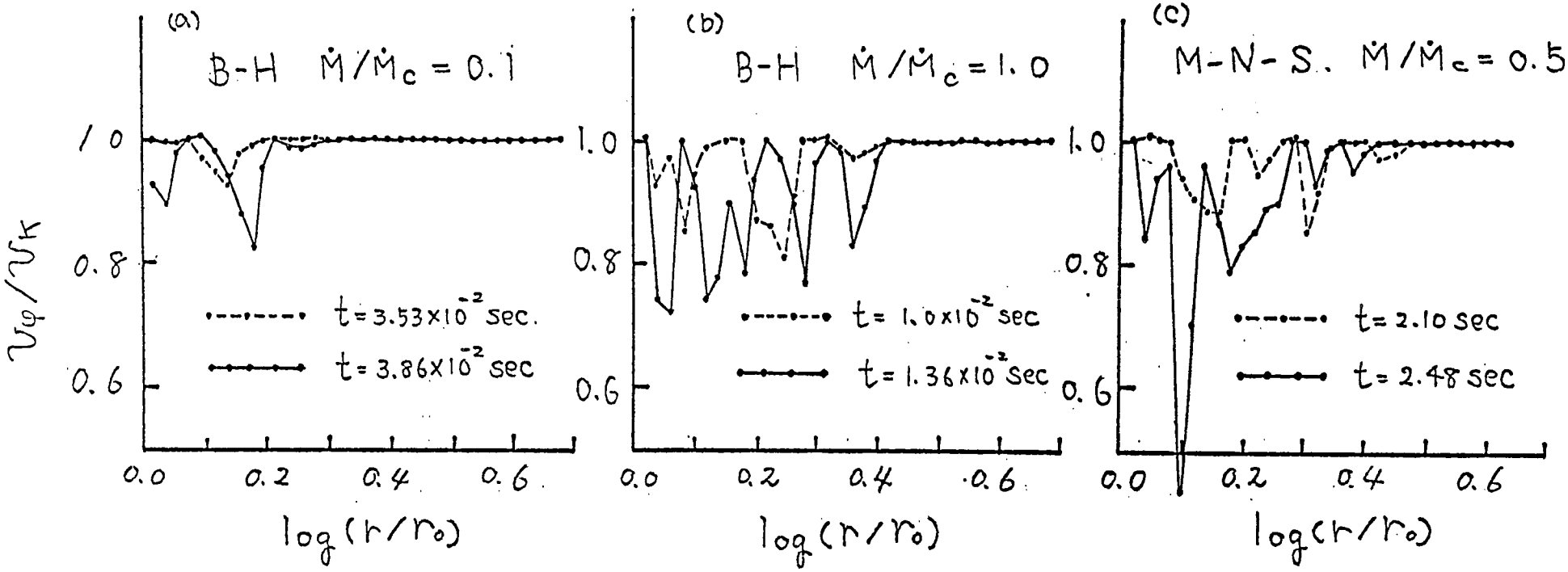
(a)
B-H $\dot{M}/\dot{M}_c = 0.1$
(b)
B-H $\dot{M}/\dot{M}_c = 1.0$
(c)
M-N-S. $\dot{M}/\dot{M}_c = 0.5$
v_φ/v_K
1.0
0.8
0.6
$t = 3.53\times10^{-2}$ sec.
$t = 3.86\times10^{-2}$ sec
$t = 1.0\times10^{-2}$ sec
$t = 1.36\times10^{-2}$ sec
$t = 2.10$ sec
$t = 2.48$ sec
0.0
0.2
0.4
0.6
$\log(r/r_0)$

Fig. 7

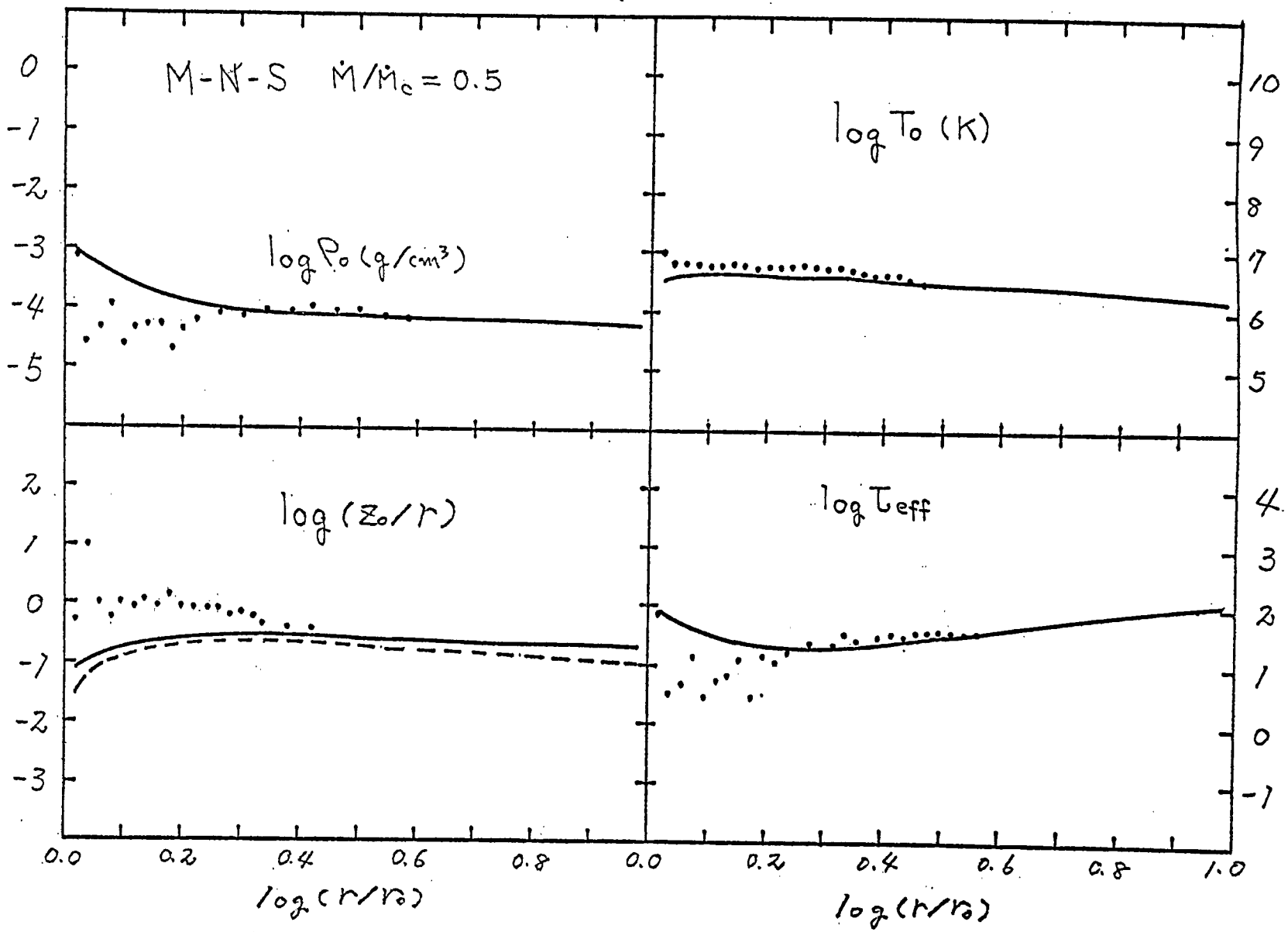
M-N-S $\dot{M}/\dot{M}_c = 0.5$
$\log P_o$ (g/cm^3)
$\log T_o$ (K)
$\log (z_o/r)$
$\log T_{eff}$
$\log (r/r_s)$
$\log (r/r_s)$

Fig 8